International Journal of Electrical Engineering.
ISSN 0974-2158 Volume 5, Number 3 (2012), pp. 335-349

http://www.irphouse.com

A Quarantine DC/DC Converter using High-Frequency Unstructured *LLC Resonant* Converter for Fuel Cell Application

[1]Dr. N.S. Sakthivel Murugan, [2]M. Murali and [3]M. Karthik

[1]Department of EEE,
Park Engineering College, Coimbatore, Tamilnadu, India
[2&3]Department of EEE,
Kuppam Engineering College,Kuppam, AP, India
E-mail: muralimunraj@gmail.com

Abstract

This paper suggests an isolated dc/dc converter using an unregulated *LLC* converter for fuel cell applications. The *LLC* converter operates as an isolated voltage amplifier with a constant voltage gain, and a nonisolated converter installed in the input stage regulates the output voltage under a wide variation of fuel cell stack voltage. By separating the functions, the unregulated *LLC* converter can be operated at an optimal switching condition, and the high-frequency operation of 300 kHz can be accomplished without introducing an excessive switching loss. The prototype converter with a 1-kW design (V_{in} = 24 ∼ 48 V/V_O = 400 V) shows an efficiency of above 90.2% under a 24-V input and full load conditions.

Index Terms: DC/DC converter, fuel cell, *LLC* converter.

Introduction

In the past century, global surface temperature has in- creased because global warming is taking place due to gas emission, such as CO_2. Aside from the global warming problem, environmental problems of air pollution, ozone de- pletion, forest destruction, and acid precipitation become worse by the combustion of fossil fuels. To prevent these effects, many activities have been evolved to reduce the fossil fuel

consumption through an increase of environmentally friendly energy supplies. Among many kinds of clean energy sources, the fuel cell is one of the most efficient energy sources that are promising in the near future [1]. It can be an alternative energy source of electrically powered devices, such as transportation, communication, computing, and residential systems. However, the fuel cell shows a large variation in output voltage under variable load conditions, and the voltage produced by the fuel cell is low in magnitude, so the voltage and the current can easily have the same order of magnitude in the applications with the output power of kilowatt range. Moreover, the low fuel cell voltage should be raised to the peak of a utility line voltage for power conditioning system design. Thus, it is necessary to design a high step-up converter with a wide line regulation performance to interface the fuel cell to various loads [2]. To achieve a high voltage gain, converters based on a transformer or coupled inductor have been considered [3]–[8]. Compared with an isolation transformer, the coupled inductor has a simple and efficient structure, but its use is restricted to applications that do not require electrical isolation. To obtain not only a high voltage gain but also the electrical isolation, current-fed converters have been widely used. Fig. 1(a) shows a two-inductor current-fed half-bridge converter. The major drawbacks of this converter are hard-switching operation and turnoff voltage spikes. To alle- viate these problems, a zero voltage switching (ZVS) technique using an active-clamp circuit can be used, but this active-clamp circuit increases the circuit complexity due to additional switch blocks [9]–[11]. The number of magnetic elements that affect the circuit volume can be reduced by using the current-fed full- bridge converter with two magnetic devices, which is shown in Fig. 1(b), but the switch blocks are increased to five, including the active-clamp circuit [12], [13]. The circuit structure can be simplified using the current-fed push–pull converter, which is shown in Fig. 1(c), but it has several disadvantages, such as the high voltage stress of the switches and low voltage conversion ratio [14]. In general, the switching frequency of the current- fed converters may be limited under several tens of kilohertz due to the switching losses. It has been reported that they are not able to come over the efficiency of 89% at a 1 kW design (V_{in} = 22 V $\sim$ 41 V/V_O = 350 V) with 100 kHz switching frequency [15]. Therefore, the additional circuitry to alleviate the voltage spikes by transformer leakage inductance and the efficiency degradation by the switching loss may be obstacles to reduce the size and cost of the current-fed converters.

In this paper, another concept of an isolated dc/dc converter is proposed for fuel cell applications. This converter is com- posed of two stages with the hard-switched boost converter for output voltage control and the unregulated *LLC* converter for electrical isolation and voltage amplification. By separating the functions, the unregulated *LLC* converter can be designed to have an optimal switching characteristic regardless of the load conditions so that the switching frequency can be increased to 300 kHz without an excessive power loss. The feasibility of the proposed converter has been verified with a 1-kW (V_{in} =24 V $\sim$ 48 V/V_O = 400 V) prototype converter.

Proposed Converter

Conditions for Unregulated Converter

Because the unregulated converter does not have any control loop, another controllable circuit is required at the input output sides, which inevitably increases the circuit complexity and volume. To avoid these problems, the unregulated converter should have the following several necessary conditions [16].

1. The switching frequency should be raised to reduce the volumes of the magnetic devices.
2. The number of magnetic elements should be minimized.
3. No snubber circuit should be used.
4. The number of switching blocks should be minimized.
5. The electrical isolation should be possible.

Fig. 2 shows the voltage-fed half-bridge and full-bridge converters. They have good characteristics, such as the ZVS of primary switches, low switch voltage stress, and small circulat- ing current. However, the voltage spikes of the secondary side of the transformer due to the resonance between the transformer leakage inductance and the diode junction capacitances are so severe that a high-voltage-rating diode and an auxiliary snubber circuit are required. It is one of the reasons of the efficiency degradation and electromagnetic interference [17]–[20]. More- over, the heavy turnoff switching loss of the primary switches may be an obstacle to increase their switching frequencies in high-current applications. Thus, they are not suitable for the use of a high-frequency unregulated converter. Fig. 3(a) shows the basic diagram of an *LLC* resonant converter. The *LLC* converter features soft switching for all load conditions, and the turnoff voltage spikes of the switches and diodes can be ab- sorbed by the input and output capacitors. This circuit structure eliminates the necessity of a snubber circuit. Fig. 3(b) shows the conventional gain characteristic of the *LLC* converter. The operational region 2 is generally used for the *LLC* converter operation because both the ZVS and zero current switching can be achieved. To use the fuel cell as an input voltage source, the *LLC* converter should be so designed that its dc gain G_{dc} is increased over two because the fuel cell output voltage is changed more than twice according to the output currents. This design produces undesirable problems, such as a large switching frequency variation, the increase of transformer size, and the heavy current stress of the switches. In addition, since the gain characteristic is affected by the quality factor Q, that is proportional to the inverse of load, it is difficult to design the converter to be operated in the region 2 in high power converters. Therefore, the *LLC* converter itself is not suitable as a dc/dc converter for fuel cell applications [21]–[23] However, the *LLC* converter is very attractive because the switching frequency can be increased without an excessive switching loss if the switching frequency is fixed to the resonant frequency and it has very simple structure with only single magnetic component. Therefore, the *LLC* converter is adequate for the unregulated converter of the proposed method

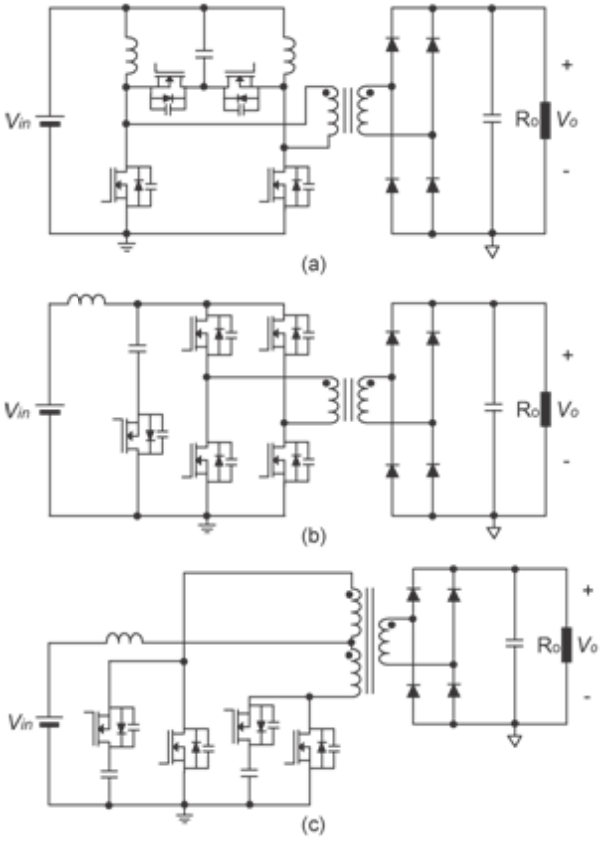

Figure 1: Current-fed-type converters with active clamp circuit. (a) Half-bridge type. (b) Full-bridge type. (c) Push–pull type

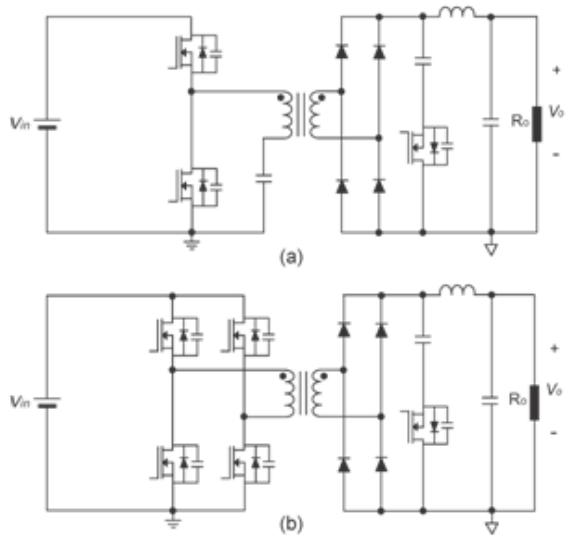

Figure 2: Voltage-fed-type converters with active clamp circuit. (a) Half-bridge type. (b) Full-bridge type.

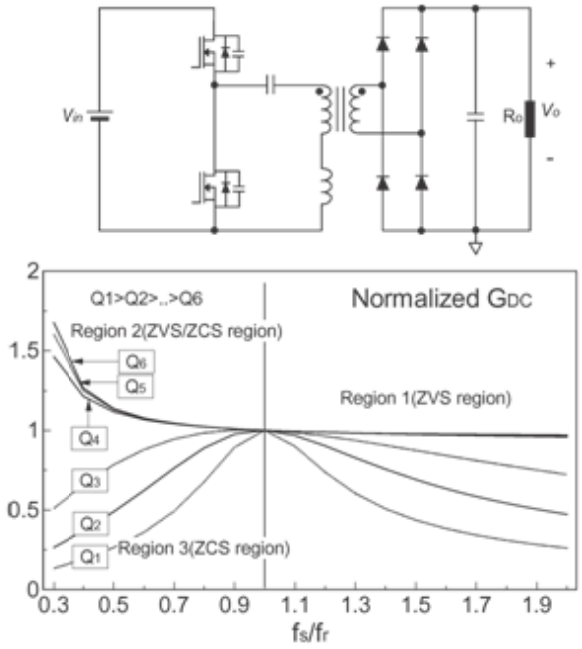

Figure 3: *LLC* resonant converter and its gain characteristics.

Proposed Converter

Fig. 4 shows two types of the proposed concept. The pre- regulator type is the cascade structure of the nonisolated con- verter, followed by the unregulated *LLC* converter, and the postregulator type has the reverse structure of the preregulator type. The lifetime of the fuel cell is seriously affected by pulsating output currents. Accordingly, the post-regulator type is not desirable because the *LLC* converter generates large pulsating resonant currents at the input stage and it increases input filter size. Fig. 5 shows the proposed converter based on the preregulator concept. The boost converter directly controls a final output voltage and the ripple current generated at the input can be alleviated through the boost inductor. By removing the feedback control loop from the *LLC* converter, the converter becomes an isolated voltage amplifier with a constant gain, and it can be operated with a minimum switching loss regardless of the input and output conditions. The link voltage V_b determines the electrical stresses and types of the switching devices located in the transformer primary side, which affects the switching and conduction losses. Because these losses are tend to move against each other according to link voltage changes, it should be optimized in the aspect of total device loss and the designed link voltage can be obtained by adjusting the voltage gain of the *LLC* converter. The method for the link voltage selection will be explained in the next section. The input-to-output rela- tionship of the proposed converter is the product of those of the boost converter and the *LLC* converter, and it can be written as

$V_b V_o \backslash^{Divided} V_{in}\ V_b$

is selected with the same value as the resonant frequency f_r to reduce the switching loss, it can be simplified by

$$V_o = V_b / V_{in} = V_b / (1 - D) = 2$$

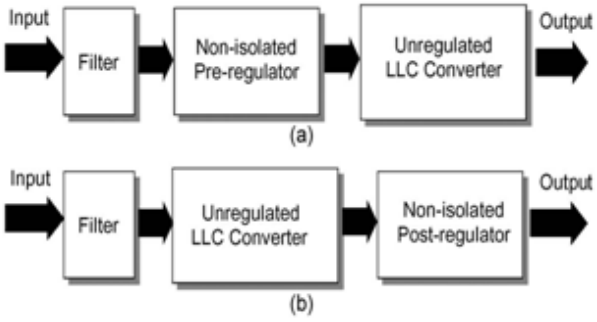

Figure 4: Two types of the proposed concept. (a) Preregulator type. (b) Post-regulator type.

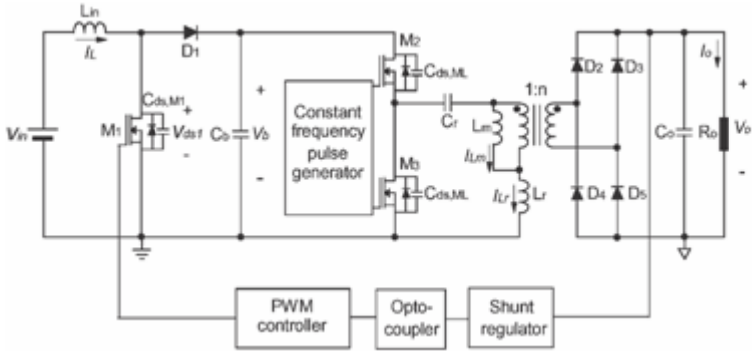

Figure 5: Schematic of the proposed converter.

Structural Comparisons between the Proposed Converter and Current-Fed Converters

Table I shows the structural comparisons between the proposed converter and the current-fed converters. The number of switch blocks of the proposed converter is not small compared with that of the basic current-fed-type converters. Considering additional active clamp circuits to absorb the voltage spikes in conventional current-fed-type converters, the proposed converter has an advantage in the switch block because it does not require any snubber circuitry. The number of magnetic elements in the proposed converter is equal or less than that of the current-fed converters. However, the proposed converter has drawbacks in the capacitor blocks and diode blocks due to the cascaded structure of the two converters. Synthesizing the comparisons, the structure of the proposed converter is not inferior to the current-fed-type converters despite of the twostage structure.-

Table 1: Structural Comparisons between the Proposed Converter and Current-Fed Converters

	Current-fed converters			Proposed converter
	Half-bridge	Full-bridge	Push-pull	
Switch block (With active clamp circuit)	2 (4)	4 (5)	2 (4)	3 (3)
Diode block (Voltage-doubler type)	4 (2)	4 (2)	4 (2)	5 (3)
Capacitor block	1	1	1	2
Inductor	2	1	1	1
Transformer	1	1	1	1

Device Loss Analysis for Link Voltage Selection

To select an optimal link voltage, it is necessary to derive a relationship between the link voltage and all of the device losses. To make a guideline to select the link voltage, we will consider only the semiconductor device losses because magnetic element losses become constant if the parameters, such as the flux swing, wire current density, core material, and operational frequency, are designed to be identical according to the link voltages. The semiconductor device loss equations can be obtained through the loss analysis of each stage and the procedure is as follows:

Boost Stage Loss Analysis

Assuming that the boost inductor is large enough to be a current source, the model and its switching waveforms can be depicted in Fig. 6. After the gate is charged to the threshold voltage Vth, the MOSFETM1 is ready to carry the current, and the gate voltage is rising from Vth to the Miller plateau level Vgs,miller. This is the linear operation level because$M$1 operates under a pinchoff state. This state continues until Vds1 reaches to 0 V. During this interval, all of the boost inductor current flows through M1 because the output diode D1 becomes to be on

OFF-state. If the base resistor Rg is small enough for the gate drive transistor to be operated in the saturation region, the turn-on gate current Ig,on can be written as

$$Ig,\text{on} = V\text{CC} - V\text{CE,sat} - V\text{gs,miller}Rg \quad (3)$$

where VCE,sat is the collector–emitter saturation voltage of n-p-n transistor Q1 and VCC is the gate drive voltage. Vgs,miller can be obtained from the transfer characteristics of M1, and a method is explained to calculate Vgs,miller from the ID–Vgs curves of the MOSFETs in [24]. The turn-on gate current determines the turn-on time of M1 Ton,B, and it can be calculated as

$$T\text{on},B = Q\text{gd}\, Ig,\text{on} \quad (4)$$

Thus, the turn-on switching loss of the boost converter can be written as follows:

$$P_{on,M1} = 1\ 2I_L(V_b - V_{on,D1})T_{on,B}f_{sB} \quad (5)$$

where $V_{on,D1}$ is the on-drop voltage of $D1$ and f_{sB} is the switching frequency of the boost converter. After V_{ds1} reaches to 0 V, the gate voltage increases to the final gate drive voltage, and $M1$ becomes completely turned on.

When the gate–source voltage is discharged to the Miller plateau level, $M1$ also enters the linear operation region, and turnoff gate current $I_{g,off}$ becomes

$$I_{g,off} = V_{EC,sat} - V_{gs,miller}R_g \quad (6)$$

In this equation, $V_{EC,sat}$ is the emitter–collector saturation voltage of p-n-p transistor $Q2$. This current charges the drain–source capacitance of $M1$, and the turnoff time of $M1$ $T_{off,B}$ is determined as follows:

$$T_{off,B} = Q_{gd}\ I_{g,off}. \quad (7)$$

Therefore, the turnoff switching loss of the boost converter is

$$P_{off,M1} = 1\ 2I_L(V_b - V_{on,D1})T_{off,B}f_{sB}. \quad (8)$$

Besides theses losses, the switching loss due to the drain–source capacitance of $M1$ $C_{ds,M1}$ and the junction capacitance of $D1$ $C_{j,D1}$ produces and it can be written as

$$P_C = (C_{ds,M1} + C_{j,D1})V\ 2b\ f_{sB}. \quad (9)$$

The conduction losses of $M1$ and $D1$ can be calculated using the rms and the average current carried by them, and they can be calculated as follows:

$$P_{con,M1} = P2oV\ inVb - V_{in}\ V_b\ R_{ds,M1} \quad (10)$$

$$P_{cond,D1} = P_oV_{on,D1}V_b \quad (11)$$

where $R_{ds,M1}$ is the on-resistance of $M1$. Therefore, the total device loss of the boost converter is as follows:

$$P_{Boost} = P_{on,M1} + P_{off,M1} + P_C + P_{con,M1} + P_{con,D1}. \quad (12)$$

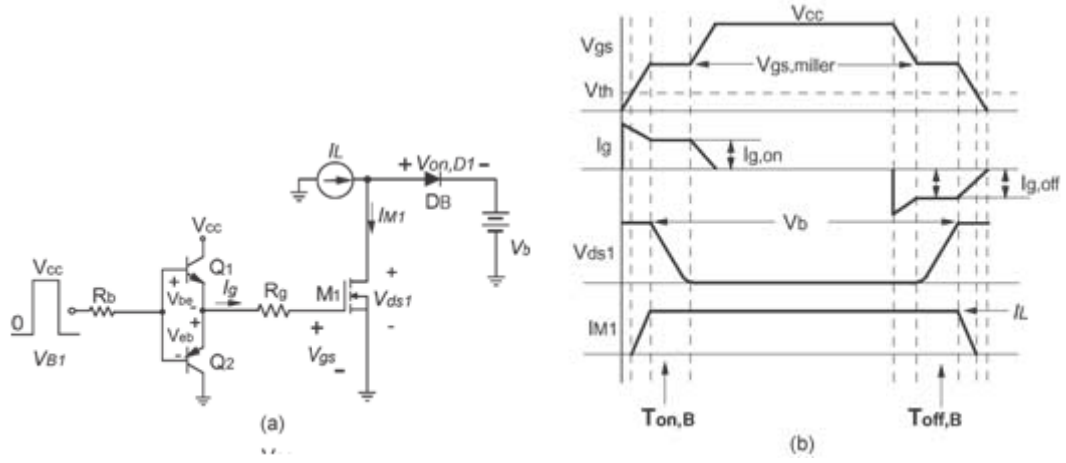

Figure 6: Boost converter model and (a) its switching waveforms (b) for loss analysis.

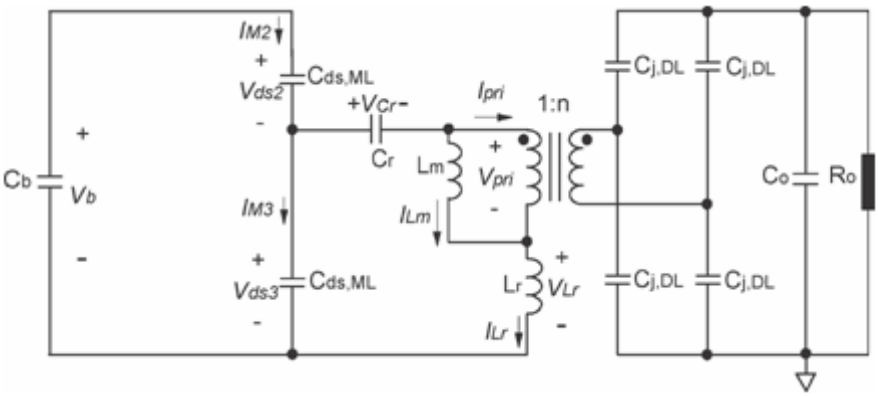

LLC Stage Loss Analysis

Before the loss analysis, it is necessary to determine L_m to accomplish the soft-switching condition. Assuming that the reverse recovery time of the output rectifier is negligible, the equivalent circuit during the dead time T_{dead} can be depicted as shown in Fig. 7. To accomplish the ZVS condition when $f_{\text{sL}} = f_r$, the peak magnetizing current $I_{Lm,\text{pk}}$ should be large enough to discharge the output capacitances of the MOSFETs and the junction capacitances of the output rectifier $D_2 \sim D_5$ during T_{dead} . This condition gives the design guideline of L_m ,

$$Lm \leq VoT\text{dead}\ 4n(2C\text{ds,ML} + 4n2Cj,\text{DL})Vbf\text{sL} \tag{13}$$

where $C_{j,\text{DL}}$ is the junction capacitance of each diode in the output rectifier and $C_{\text{ds,ML}}$ is the drain–source capacitance of M_2 or M_3. Equation (13) guarantees the ZVS condition of the switches, and the loss analysis is performed with the assumption that L_m is designed to meet this inequality. Fig. 8 is the switching waveform of the unregulated *LLC* converter. When M_2 enters turn-off transition, it experiences the linear operation region during the gate pulse passes through the Miller plateau level and V_{ds2} is linearly increased. Because the slope of V_{ds2} determines that of V_{ds3} , the discharging current of the drain–source capacitance of M_3 can be calculated as

$$IM3 = -C\text{ds,ML}\ Vb\ T\text{off},L. \tag{14}$$

The turnoff time of $M2$ $T\text{off},L$ can be calculated with (7).

Therefore, the current flowing through the channel of $M2$ can be obtained as

$$IM2 = ILr + IM3$$
$$= ILm,\text{pk} + IM3 = Vo4nLmf\text{sL} - C\text{ds,ML}VbT\text{off},L. \tag{15}$$

With this equation, the switching loss of $M2$ can be written as (16) by assuming that ILr is linearly decreased during the dead time

$$P\text{off},M2 = 16Vb\_Vo4nLmf\text{sL} - C\text{ds,ML}VbT\text{off},L\_T\text{off},Lf\text{sL}. \tag{16}$$

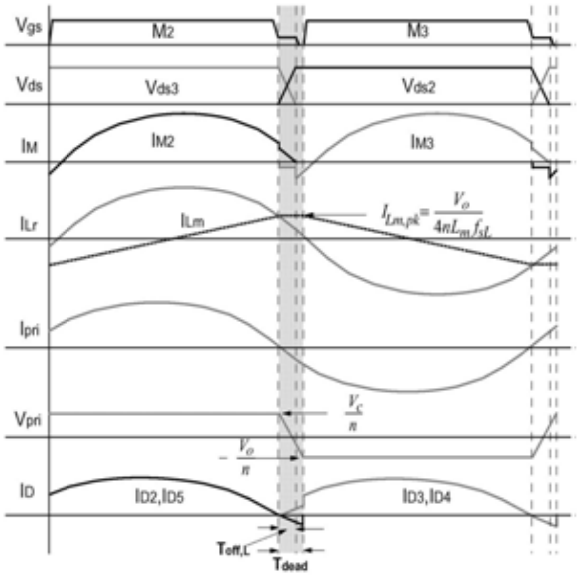

Figure 8: Switching waveforms of the unregulated *LLC* converter

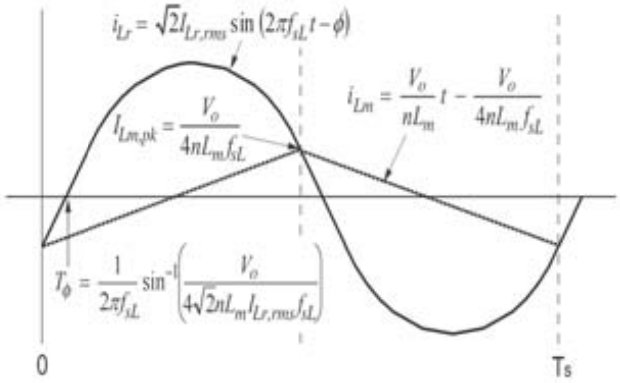

Figure 9: Resonant current waveform and its key expressions.

The same turnoff loss happens at $M3$, so the total turnoff loss of the MOSFETs can be found as follows:

Poff,SW =13Vb_Vo4$nLmf$sL− Cds,MLVbToff,$L_T$off,LfsL. (17)

Because $M2$ and $M3$ show ZVS operation, (17) becomes the total switching loss of the MOSFETs. Fig. 9 shows the reso- nant current waveform and its key expressions. The difference between the resonant current and the magnetizing current is transferred to the load, and it can be expressed as

2fsn1/_(2fsL)0(iLr − im) dt = VoRo . (18)

With (18) and the expressions of iLr and iLm in Fig. 9, the rms value of the resonant current can be obtained as follows:

ILr,rms =Square root of (2*PoVb_R2o*32*n*4*L*2*mf*2sL+π28) (19)

Table II: Loss Equations for Link Voltage Selection

	Loss equations
Boost FET loss	$\frac{1}{2}I_L(V_b - V_{on,D1})(T_{on,B} + T_{off,B})f_{sB} + C_{ds,M1}V_b^2 f_{sB} + \left(\frac{P_o^2}{V_{in}^2}\frac{V_b - V_{in}}{V_b}\right)R_{ds,M1}$
Boost diode loss	$C_{j,D1}V_b^2 f_{sB} + \frac{P_o V_{on,D1}}{V_b}$
LLC FET loss	$\frac{1}{3}V_b\left(\frac{V_o}{4nL_m f_{sL}} - C_{ds,ML}\frac{V_b}{T_{off,L}}\right)T_{off,L}f_{sL} + \left(\frac{2P_o}{V_b}\sqrt{\frac{R_o^2}{32n^4L_m^2 f_{sL}^2} + \frac{\pi^2}{8}}\right)^2 R_{ds,ML}$
LLC output rectifier loss	$\frac{2P_o}{V_o}V_{on,DL}$

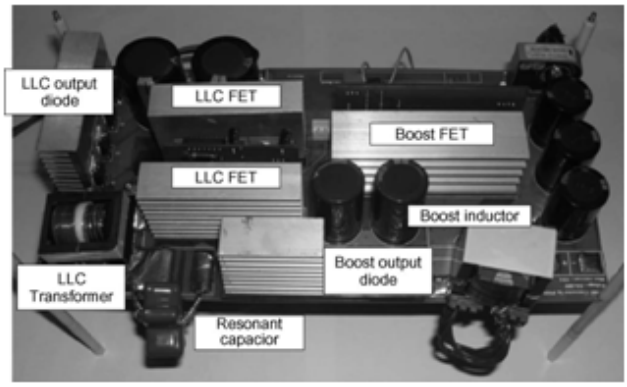

Figure 10: Photograph of the prototype converter.

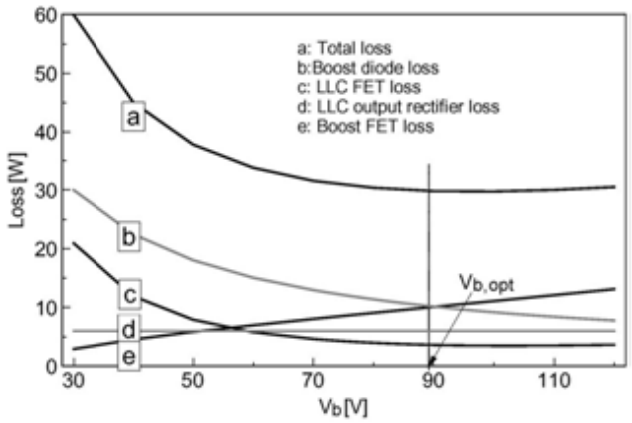

Figure 11: Calculated semiconductor device losses according to the link voltages at V_{in} = 24 V.

Table III: Actual Parameters for Loss Calculation

Parameter	Value	Parameter	Value	Parameter	Value
$C_{ds,M1}$	820pFX3	V_{in}	24V	L_m	5μH
$R_{ds,M1}$	7.6mΩ/3	V_o	400V	n	11
$V_{on,D1}$	0.9V	P_o	1kW	$T_{on,B}$	17.2ns
$C_{j,D1}$	200pFX2	R_o	160Ω	$T_{off,B}$	34.5ns
$C_{ds,ML}$	820pFX2	I_L	50A	$T_{off,L}$	37.5ns
$R_{ds,ML}$	7.6mΩ/2	f_{sB}	50kHz		
$V_{on,DL}$	1.2V	f_{sL}	300kHz		

Accordingly, the total conduction loss happened at *M*2 and *M*3 can be calculated as

$$P\text{con,SW} = 2PoVb\_R2o32n4L2mf2\text{sL} + \pi 28\text{-}2R\text{ds,ML} \quad (20)$$

where *R*ds,ML is the on-resistance of *M*2 or *M*3. Because the output rectifier has only the conduction loss due to zero-voltage and zero-current-switching operation, its loss expression is written as

$$P\text{con,REC} = 2PoVo\ V\text{on,DL} \quad (21)$$

where *V*on,DL is the on-drop voltage of each diode in the output rectifier. Therefore, the total device loss of the *LLC* converter is

$$P\text{loss,LLC} = P\text{off,SW} + P\text{con,SW} + P\text{con,REC}. \quad (22)$$

The loss equations to select the link voltage are rearranged in Table II. By performing the partial derivative of these loss equations with respect to *Vb*, the optimal link voltage *Vb,*opt can be obtained with selected device parameters. Based on the calculated value of *Vb,*opt, some adjustment should be performed, considering the device voltage ratings and power losses.

Experimental Results

The proposed converter has been designed with a 1-kW output power (400 V/2.5 A) at *V*in = 24–48 V, and the prototype hardware is shown in Fig. 10. The selected switching devices in this design are *M*1 = FDP3632 × 3, *M*2 = *M*3 = FDP3632 ×2, *D*1 = V60100C × 2, and *D*2 ∼ *D*5 = CD06060.

As shown in Fig. 11 and as depicted with the loss equations in Table II and the actual parameters listed in Table III, *Vb,*opt is calculated at about 90 V from the selected devices at *f*sB = 50 kHz and *f*sL = 300 kHz. Considering voltage-rating margins, *Vb* is finally selected as 73 V. Using the selected link voltage, the transformer turn ratio is calculated as 1:11 from (2), and the transformer is constructed with EER3542 ferrite core (3T:33T).Since the transformer has a leakage inductance of 1.3 μH, 0.216 μF is selected for *Cr* to make *fr* equal to *f*sL. With these designed parameters and with *T*dead = 160 ns, the maximum *Lm* is calculated as 5.2

μH from (13), and 5 μH is used in this design. The inductor uses 20 μH, and it is implemented with a PQ4040 ferrite core. Fig. 12 shows the operational waveforms of the boost converter and *LLC* converter under V_{in} = 24 and 48 V at a full load condition. This figure shows that the *LLC* converter is operated with a fixed frequency of 300 kHz and that the output regulation can be accomplished only by the duty control of the boost converter switch. Fig. 13 is the measured resonant waveforms of the unregulated *LLC* converter under load changes. The resonant currents maintain the same wave shape except for their magnitudes according to load conditions, which maintains the soft-switching condition of the *LLC* switches under all load changes. This characteristic gives a good efficiency at a light load where the efficiency is degraded by the switching loss. Fig. 14 is the experimental setup with a Nexa fuel cell stack. This fuel cell stack provides 1.2 kW of net output power, and the output voltage varies with power, ranging from about 43 V when the system is idle to about 26 V at a full load. To test the dynamic performance, a grid-tied inverter, which delivers the power generated by a fuel cell stack to a grid, is connected at the output of the proposed converter. Fig. 15 shows the test results with the Nexa fuel cell stack, and Fig. 16 shows the transient responses under load changes. They show that the converter regulates the output voltage well under wide fuel cell stack voltage and load changes. The measured efficiency is depicted in Fig. 17. As predicted through loss analysis, the efficiency becomes degraded as the link voltage becomes increased. As shown in this figure, the efficiency of V_b = 85 V is better than that of V_b = 73 V which is selected for the prototype design, but there is no voltage margin in the semiconductor devices located at the low voltage side due to voltage spikes. At a 24-V input and at the maximum load conditions, the efficiency of the boost converter is 95.5%, and that of the *LLC* converter is 94.5%. The resulting efficiency becomes 90.2%. Despite the high-frequency operation of the *LLC* converter, the efficiency has been recorded to be around 94% at light and/or medium load ranges

Conclusion

A high-frequency isolated dc/dc converter for fuel cell applications has been proposed in this paper. It is composed of the boost converter for output voltage regulation and the isolated voltage amplifier using the unregulated *LLC* converter. To select an optimal link voltage for efficiency improvement, design equations have been derived through performing a de- vice loss analysis. From the experimental results from the 1-kW prototype converter that has been designed with switch- ing frequencies of 50 kHz in the boost stage and 300 kHz in the *LLC* stage, an efficiency of more than 90.2% has been obtained at a 24-V input. Another advantage of the proposed converter is that the efficiency is high at light and medium load ranges because the switching loss is small. Therefore, it is suitable for fuel cell applications requiring a high voltage gain and stable regulation performance under wide fuel cell voltage changes. Moreover, this converter can be easily applied to bidirectional converters because the unregulated *LLC* resonant converter has a bidirectional power flow according to the input and output conditions.

References

[1] W. Jiang and B. Fahimi, "Active current sharing and source management in fuel cell battery hybrid power system," *IEEE Trans. Ind. Electron.*, vol. 57, no. 2, pp. 752–761, Feb. 2010.

[2] S. V. Araujo, R. P. Torrico-Bascopé, and G. V. Torrico-Bascopé, "Highly efficient high step-up converter for fuel-cell power processing based on three-state commutation cell," *IEEE Trans. Ind. Electron.*, vol. 57, no. 6, pp. 1987–1997, Jun. 2010.

[3] T. F. Wu, Y. S. Lai, J. C. Hung, and Y. M. Chen, "Boost converter with coupled inductors and buck boost type of active clamp," *IEEE Trans. Ind. Electron.*, vol. 55, no. 1, pp. 154–162, Jan. 2008.

[4] S. K. Changchien, T. J. Liang, J. F. Chen, and L. S. Yang, "Novel high step-up dc–dc converter for fuel cell energy conversion sys- tem," *IEEE Trans. Ind. Electron.*, vol. 57, no. 6, pp. 2007–2017, Jun. 2010.

[5] J. Y. Lee and S. N. Hwang, "Non-isolated high-gain boost converter using voltage-stacking cell," *Electron. Lett.*, vol. 44, no. 10, pp. 644–645, May 2008.

[6] L. S. Yang, T. J. Liang, and J. F. Chen, "Transformerless dc/dc converters with high step up voltage gain," *IEEE Trans. Ind. Electron.*, vol. 56, no. 8, pp. 3144–3151, Aug. 2009.

[7] W. Li and X. He, "High step-up bidirectional isolated converter with two input power sources," *IEEE Trans. Ind. Electron.*, vol. 236, no. 4, pp. 1791–1801, Jul. 2008.

[8] D. Wang, Y. Deung, and X. He, "Isolated ZVT boost converter with switched capacitors and coupled inductors," in *Proc. IECON*, 2008, pp. 808–814.

[9] J. M. Kwon and B. H. Kwon, "High step-up active-clamp converter with input-current doubler and output-voltage doubler for fuel cell power systems," *IEEE Trans. Power Electron.*, vol. 24, no. 1, pp. 108–115, Jan. 2009.

[10] S. K. Han, H. K. Yoon, G. W. Moon, and M. J. Youn, "A new ac- tive clamping zero-voltage switching PWM current-fed half-bridge con- verter," *IEEE Trans. Power Electron.*, vol. 20, no. 6, pp. 1271–1279, Nov. 2005.

[11] Y. Lembeye, V. D. Bang, G. Lefèvre, and J. P. Ferrieux, "Novel half-bridge inductive dc–dc isolated converters for fuel cell applications," *IEEE Trans. Energy Convers.*, vol. 24, no. 1, pp. 203–210, Mar. 2009.

[12] A. Averberg, K. R. Meyer, and A. Mertens, "Current-fed full bridge converter for fuel cell systems," in *Proc. Power Electron. Spec. Conf.*, 2008, pp. 866–872.

[13] X. Kong and A. M. Kambadkone, "Analysis and implementation of a high efficiency, interleaved current-fed full-bridge converter for fuel cell system," *IEEE Trans. Power Electron.*, vol. 22, no. 2, pp. 543–550, Mar. 2007.

[14] C. L. Chu and C. H. Li, "Analysis and design of a current-fed zero- voltage-switching and zero-current-switching CL-resonant push–pull dc–dc converter," *IET Power Electron.*, vol. 2, no. 4, pp. 456–465, Jul. 2009.

[15] A. K. Rathore, A. K. S. Bhat, and R. Oruganti, "A comparison of soft-switched dc–dc converters for fuel cell to utility interface application," in *Proc. PCC*, 2007, pp. 588–594.

[16] R. Ridley, "The incredible shrinking power supply," *Switching Power Mag.*, pp. 1–6, 2005. [Online]. Available: http://www.switchingpowermagazine.com/topologies.aspx

[17] J. A. Sabate, V. Vlakovic, R. B. Ridley, F. C. Lee, and B. H. Cho, "Design considerations for high-voltage high-power full-bridge zero-voltage-switched PWM converter," in *Proc. APEC*, 1990, pp. 275–284.

[18] L. H. Mweene, C. A. Wright, and M. F. Schlecht, "A 1 kW, 500 kHz front-end converter for a distributed power supply system," in *Proc. APEC*, 1989, pp. 423–432.

[19] M. L. Heldwein, A. F. de Souza, and I. Barbi, "A primary side clamping circuit applied to the ZVS-PWM asymmetrical half-bridge converter," in *Proc. Power Electron. Spec. Conf.*, 2000, pp. 199–204.

[20] T. Mishima and M. Nakaoka, "Performance evaluation on a fixed- frequency ZCS-PWM asymmetrical half-bridge dc–dc converter with auxiliary active edge-resonant snubber," in *Proc. Power Electron. Spec. Conf.*, 2008, pp. 2177–2183.

[21] A. K. Bhat, "Analysis and design of *LC L*-type series resonant converter," *IEEE Trans. Ind. Electron.*, vol. 41, no. 1, pp. 118–124, Feb. 1994.

[22] K. Jin and X. Ruan, "Hybrid full-bridge three-level *LLC* resonant converter—a novel dc–dc converter suitable for fuel-cell power system," *IEEE Trans. Ind. Electron.*, vol. 53, no. 5, pp. 1492–1503, Oct. 2006

[23] K. H. Yi and G. W. Moon, "Novel two-phase interleaved *LLC* series- resonant converter using a phase of the resonant capacitor," *IEEE Trans. Ind. Electron.*, vol. 56, no. 5, pp. 1815–1819, May 2009.

[24] Estimating MOSFET Parameters From the Datasheet, Texas Instrument Seminar Topics Slup170, 2002. [Online]. Available: http://focus.ti.com/lit/ml/slup170/slup170.pdf